Development and evaluation of the IRIS–OPTIscanner, a general–purpose optical tomographic imaging system

Randall L. Barbour[1,2], Randy Andronica[3], Quan Sha[1], Harry L. Graber[1] and Ira Soller[3]

[1]Department of Pathology, SUNY Health Science Center at Brooklyn

[2]Department of Electrical Engineering, Polytechnic University

[3]Scientific and Medical Instrumentation Center, SUNY Health Science Center at Brooklyn

Abstract

We have constructed a general purpose optical tomographic imaging device capable of evaluating a variety of body appendages. A novel functional feature of the instrument is its use of a geometrically *adaptive* scanning head, in the form of a mechanical iris, about which are attached optical fibers positioned in a circular array. By adjusting the pass–through diameter of the iris, optical fibers can be brought into gentle contact with a tissue target. This serves to improve optical coupling while simultaneously stabilizing the tissue against motion artifacts. In addition, in many instances it also permits gentle deformation of the tissue to a simple circular geometry which is favorable for data analysis. The instrument also employs a rotating filter array that serves to extend the dynamic range of measurement to $>10^{12}$ while retaining excellent precision (CV = 0.2–0.3%). Reconstruction results of laboratory phantoms and physiological imaging studies of the human forearm are presented.

Introduction

In recent years, the possibility of acquiring tomographic images of thick tissue structures from measurements performed in the NIR region has caught the attention of many [1,2]. Fueling this interest is the recognition of the significant cost, portability and sensitivity advantages that NIR measurements offer in comparison to established imaging methods (*e.g.*, MRI, CT, SPECT, PET). Until now, much of the development effort has been focused on algorithm refinement. Much progress appears to have been made, at least with analysis of computed data and measurements with simply structured laboratory phantoms [3–6]. Lagging has been serious attempts to develop practical clinical systems. Extension of measurement strategies suitable for evaluation of solid phantoms to clinical situations is not straightforward.

It is evident that tissue structures come in many geometries and are prone to motion artifacts. Accurate knowledge of external tissue geometry at the time of measurement may prove important, as many of the reconstruction methods currently proposed (*i.e.*, perturbation methods) require some form of comparative analysis to a defined reference state. It is well known that these methods can produce unstable solutions should the initial guess be severely inaccurate, which certainly could be the case in the absence of accurate knowledge of tissue geometry. This dilemma may prove problematic, as the external geometry of tissue is basically arbitrary and is not conveniently measured. It follows that it would be useful to adopt measurement strategies that obviate the criticality of prior knowledge of tissue geometry.

One approach would be to immerse the target tissue in an index–matching scattering fluid, thereby effectively extending the external boundary of the tissue. While potentially practical, this strategy effects a non–contact measurement, rendering it susceptible to motion artifacts. Attention to the latter is almost certainly necessary given that tissue attenuates light exponentially. Beyond this, the presence of an intervening scattering medium will certainly add to the measured attenuation and further reduce available resolution.

An alternative methodology would be to perform a contact measurement. While this likely would enable collection of improved signal levels it would not by itself necessarily resolve the geometry problem nor even the problem of motion artifacts. In principal, both could be simultaneously addressed by confining tissue to a fixed apparatus. This also it not without its limitations, given the range of tissue sizes and desirability of preserving a large view angle. The approach we have pursued has been to consider a design that would serve to: i. mechanically stabilize

OSA TOPS Vol. 21 Advances in Optical Imaging and Photon Migration, James G. Fujimoto and Michael S. Patterson (eds.)

tissue, ii. bring optical fibers into direct tissue contact, iii. be geometrically *adaptable* to accommodate a range of tissue sizes. To this end we have incorporated a mechanical iris into the scanner head, about which optical fibers are attached in a circular array. Adjustment of the pass–through diameter of the iris causes the translation of the fibers in a radial direction. The device, shown in Figure 1, presently incorporates 18 fiber bundles, each serving to transmit and receive light. The current design allows for continuous adjustment of the iris opening over a diameter range of 3–15 cm. Other components of the system include a servo–controlled input multiplexer, an adjustable filter array that enables measurements over a large dynamic range, and a output coupler that couples the detector fibers to a CCD camera.

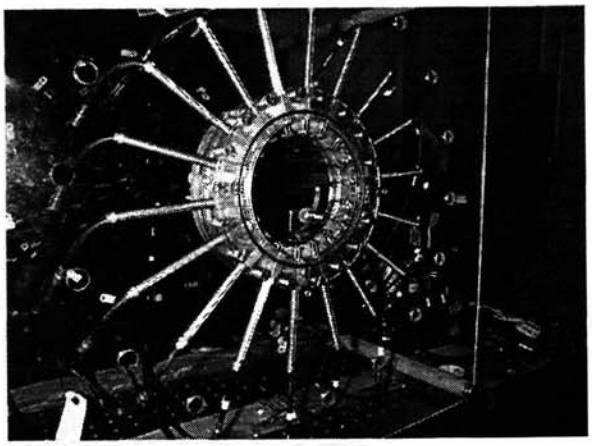

Figure 1 Photograph of iris and 18 attached sending/receiving optical fiber bundles.

Apart from the above considerations, the iris design would appear well–suited for optical measurements of tissue, as the unit also is capable of gently compressing tissue, causing it to assume a circular geometry. While skeletal features can restrict this capability, in certain cases we have found that the iris design readily permits examination of many features of the arms, the legs, and, the breast. In the breast case, the distendability of the tissue should allow for even greater compression should the need arise. Compared to planar compression techniques, radial compression has the added advantage of preserving view angle. The axial measurement geometry of the iris readily permits extension in the direction normal to the measurement plane. This is easily accomplished by arranging several iris units in parallel to form a stack, each of which whose openings is independently adjustable. This allows for specific contouring to different tissue sizes, facilitating interrogation of 3–D volumes.

Results

I. Calibration and Stability Studies

Figure 2 shows results of measurements determining the relative coupling efficiency of each optical fiber bundle. This measurement determines the efficiency with which light propagates through the system, normalized to the mean value of all the fibers.

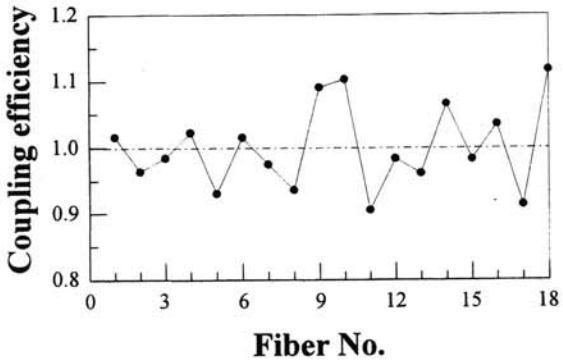

Figure 2 Optical fiber coupling efficiency.

Basically, light from a laser diode (780 nm) is directed to the input end of an 1–mm–diameter fiber that terminates at the opening of the iris. Light exiting from a target is collected by a total of 18 fiber bundles positioned at 20° intervals around the target. The collected light is then delivered to an adjustable filter assembly which contains a multi–segmented filter wheel designed to enable complete 360° simultaneous measurement from a target. Light

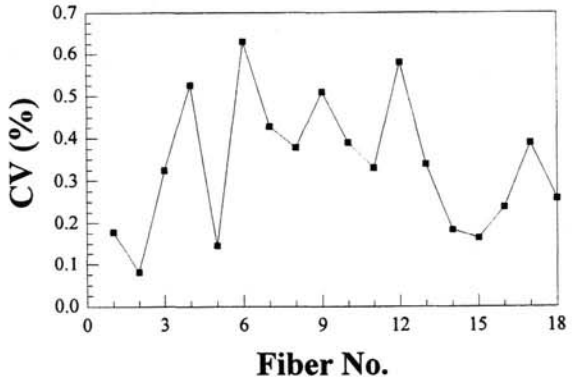

Figure 3 Measurement precision.

passing through the filters is collected by receiving bundles and directed to a CCD camera. Presently,

the latter is accomplished by optical coupling. Use of a fiber taper is currently being incorporated.

Determination of the precision of measurement for each fiber bundle is shown in Figure 3. It can be seen that the coefficient of variation (CV) of measurement varies between <0.1–0.6%, with an average value of approximately 0.3% (n=5). Data were collected from a 9–cm–diameter delrin rod.

II. Tomographic imaging studies with laboratory phantoms.

Tomographic measurements were performed on three different laboratory phantoms: a homogeneous solid delrin rod measuring 9 cm in diameter, and two different arrangements of 2–mm–diameter black polyethylene tubing surrounding a brass rods. In one case two rods were present, four in the other. In the latter two cases, the rod assemblies were placed inside a latex laboratory glove filled with 1% Intralipid®. This was used to mimic the deformability of tissue. The assembly was then placed inside the iris, and the iris diameter adjusted until all fibers were in gentle contact (final dia. approx. 7 cm). Reconstructed images of these phantoms are shown in Figures 4–6. Data analysis was based on evaluation of an 18×18 data set (324 source–detector pairs) using a previously described iterative backprojection algorithm for perturbations in the absorption coefficient [7]. Figure 4 shows the image quality achieved from the delrin rod. The result is

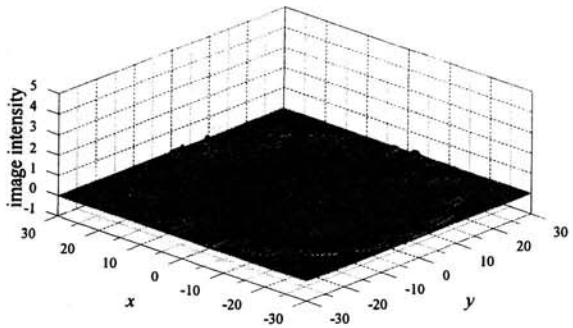

Figure 4 Reconstructed image of homogeneous delrin rod, relative to itself (*i.e.*, noise image).

essentially flat throughout the plane, with the exception of a boundary artifact associated with the source location. Data in Figures 5–6 are images of the laboratory glove containing 2 and 4 inclusions. With the exception of failing to resolve the two rods

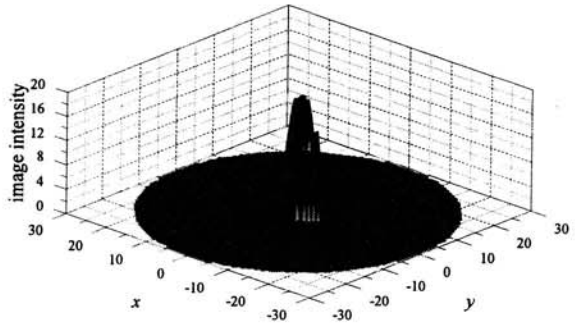

Figure 5 Reconstructed image of 2–rod phantom, relative to homogeneous reference medium.

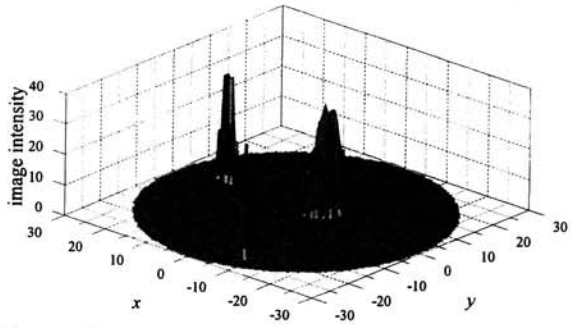

Figure 6 Reconstructed image of 4–rod phantom, relative to homogeneous reference medium.

positioned within 1.5 cm of each other (central region), the quality of the reconstructions are excellent. In both instances the solutions obtained were essentially free of any artifacts (positivity constraint used), and peak location had a maximum $x + y$ error of < 2 mm. In the case of the two rods located near the center, the position considered was the midpoint between them.

III. Physiological Imaging Studies of the Human Forearm.

Our principal objectives for these early studies was to ascertain the sensitivity and repeatability of measurement given a simple physiological perturbation. Two different protocols were followed, both involving tomographic measurements on the mid–forearm of a volunteer. In the first case we measured the difference in signal strengths obtained during a finger–flexor study. For each source position, measurements were made with the hand in the open and closed positions. The difference signals were stored and subsequently analyzed. Two separate sets of measurements were made and the reconstructed images are shown in Figures 7 and 8.

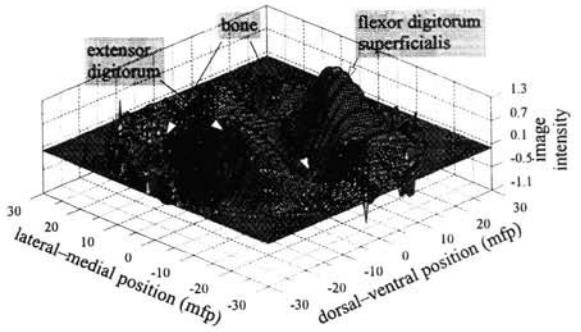

Figure 7 Image reconstructed from first set of finger–flexor measurements (target = forearm when fingers are flexed, reference = forearm when fingers are extended), with tentative identification of image peaks with anatomical structures.

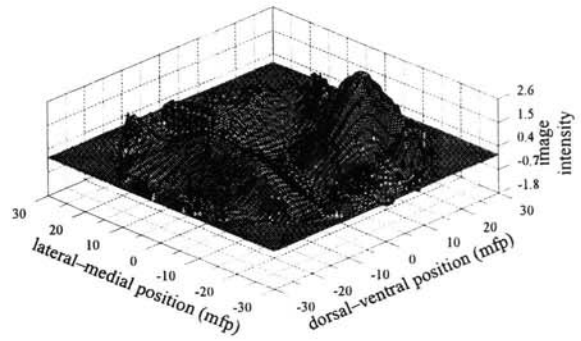

Figure 8 Image reconstructed from second set of finger–flexor measurements.

In the second experiment, a pressure cuff was place on the upper arm and inflated to 20 and 50 mm Hg. For these studies an initial set of measurements were performed without the cuff inflated, immediately followed by measurements with the indicated pressure. As with the finger–flexor study, the measured difference signal was evaluated. The reconstructed images are shown in Figures 9 and 10.

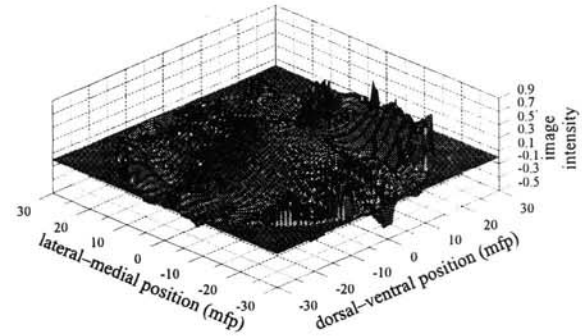

Figure 9 Image reconstructed from first set of pressure cuff measurements (target = forearm when cuff is inflated to 20 mm Hg, reference = forearm when cuff is deflated).

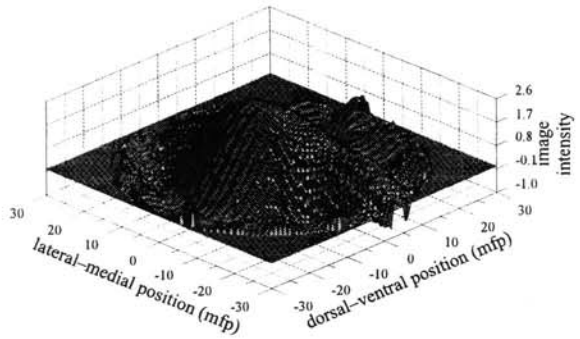

Figure 10 Image reconstructed from first set of pressure cuff measurements (target = forearm when cuff is inflated to 50 mm Hg, reference = forearm when cuff is deflated).

Discussion

In this report we have described the design and initial performance results of a novel geometrically adaptive tomographic imaging device well suited for investigation of a variety of body appendages. A key feature of the unit is a mechanical iris that serves to bring optical fibers into gentle contact with the tissue. While adjustable, the unit is mechanically quite stable at any pass–through diameter and is very effective in stabilizing the tissue against motion artifacts. Precision studies showed that the overall error of measurement was approximately 0.3% for light propagating through the entire system. While this is good, it is believed that much better performance can be achieved by using a fiber taper to couple light form the fibers to the CCD camera. In addition, further improvements can be made by adding a reference measurement and by using index matching fluid at the various interfaces whenever possible.

Results of phantom imaging studies are encouraging. The three cases examined, a homogeneous rod, two inclusions and four inclusions, all produced good quality results. Further improvements are expected by better matching of boundary conditions, and by computing perturbations in absorption and scattering simultaneously.

Results of the forearm studies are all also quite encouraging, but it is necessarily more difficult to render definitive interpretation. The anatomic assignments listed in Figures 6 and 7 were made based on the expected movement of muscle groups in

the flexor study and known orientation of the arm in the apparatus. Recall that the computed image is a difference image based on measured values. In this regard it should not be expected that the structures seen would coincide as what would be expected by, say, MRI. No doubt definitive validation of these assignments will require much more careful study.

Putting aside these issues, there are specific features in the images that are noteworthy. First is the remarkable repeatability of the computed image. It deserves emphasizing that these images were derived from measurements made several hours apart, each requiring new subject setups with the apparatus. Second, we note that all incidences of high spatial frequencies are limited to the boundary. The features in the interior are all smooth. Similar results were obtained with the pressure cuff study. Definitive interpretation of these images is also difficult at this time. Nevertheless there are two significant features in the images. The first deals with the appearance of a broad peak in the middle of the image. We interpret this as pooling of blood in the core of the arm. This result is expected given the nature of the perturbation. The second is a quantitative observation. The maximum amplitude of the image at 20 mm Hg is approximately 25% that of the image at 50 mm Hg. This result coincides well with the observation that the maximal relative intensity change determined by measurement was approximately 25% for the former and >90% for the latter case. This finding also emphasizes the significant sensitivity the measurement has to variations in tissue hemodynamics.

Acknowledgments: This grant was support in part by NIH grant CA66184–A02.

References

[1] *OSA Tends in Optics and Photonics on Advances in Optical Imaging and Photon Migration*, R. R. Alfano, J. G. Fujimoto, eds., (Optical Society of America, Washington, DC 1996), Vol. 2.

[2] *Optical Tomography and Spectroscopy of Tissue: Theory, Instrumentation, Model, and Human Studies II*, B. Chance, R. R. Alfano, eds., Proceedings of SPIE Vol. 2979 (1997).

[3] M. Schweiger, S. R. Arridge, D. T. Delpy, "Application of the finite–element method for the forward and inverse models in optical tomography," *J. Mathematical Imaging and Vision*, Vol. 3, pp. 263–283 (1993); J. C. Hebden, S. R. Arridge, "Imaging through scattering media by the use of an analytical model of perturbation amplitudes in the time domain," *Applied Optics*, Vol. 35, pp. 6788–6796 (1996).

[4] M. A. O'Leary, D. A. Boas, B. Chance, A. G. Yodh, "Experimental images of heterogeneous turbid media by frequency–domain diffusing–photon tomography," *Optics Letters*, Vol. 20, pp. 426–428 (1995); X. D. Li, T. Durduran, A. G. Yodh, B. Chance, D. N. Pattanayak, "Diffraction tomography for biomedical imaging with diffuse–photon density waves," *Optics Letters*, Vol. 22, pp. 573–575 (1997).

[5] H. Jiang, K. D. Paulsen, U. L. Österberg, "Optical image reconstruction using DC data: simulations and experiments," *Physics in Medicine and Biology*, Vol. 42, pp. 1483–1498 (1996); H. Jiang, K. D. Paulsen, U. L. Österberg, B. W. Pogue, M. S. Patterson, "Optical image reconstruction using frequency–domain data: simulations and experiments," *J. Optical Society of America A*, Vol. 13, pp. 253–266 (1996); H. Jiang, K. D. Paulsen, U. L. Österberg, M. S. Patterson, "Frequency–domain optical image reconstruction in turbid media: an experimental study of single–target detectability," *Applied Optics*, Vol. 36, pp. 52–63 (1997).

[6] J. Chang, H. L. Graber, R. L. Barbour, R. Aronson, "Recovery of optical cross–section perturbations in dense–scattering media by transport–theory–based imaging operators and steady–state simulated data," *Applied Optics*, vol. 35, pp. 3963–3978 (1996); Y. Yao, Y. Wang, Y. Pei, W. Zhu, R. L. Barbour, "Frequency–domain optical imaging of absorption and scattering distributions by a Born iterative method," *J. Optical Society of America A*, Vol. 14, pp. 35–342 (1997); W. Zhu, Y. Wang, Y. Deng, Y. Yao, R. L. Barbour, "A wavelet–based multiresolution regularized least squares reconstruction approach for optical tomography," *IEEE Transactions on Medical Imaging*, Vol. 16, pp. 210–217 (1997).

[7] H. L. Graber, J. Chang, J. Lubowsky, R. Aronson, R. L. Barbour, "Near infrared absorption imaging of dense scattering media by steady–state diffusion tomography," in *Photon Migration and Imaging in Random Media and Tissues*, B. Chance, R. R. Alfano, eds., Proceedings of SPIE Vol. 1888, pp. 372–386 (1993).